Nanofiber-based high-Q microresonator for cryogenic applications

JOHANNA HÜTNER,[1] THOMAS HOINKES,[1] MARTIN BECKER,[2] MANFRED ROTHHARDT,[2] ARNO RAUSCHENBEUTEL,[1,3,4] AND SARAH M. SKOFF[1,5]

[1] *Vienna Center for Quantum Science and Technology, Atominstitut, Technische Universität Wien, Stadionallee 2, 1020 Vienna, Austria*
[2] *Institute of Photonic Technologies IPHT, Albert-Einstein-Strasse 9, 07745 Jena, Germany*
[3] *Department of Physics, Humboldt-Universität zu Berlin, 10099 Berlin, Germany*
[4] *arno.rauschenbeutel@hu-berlin.de*
[5] *sarah.skoff@tuwien.ac.at*

Abstract: We demonstrate a cryo-compatible, fully fiber-integrated, alignment-free optical microresonator. The compatibility with low temperatures expands its possible applications to the wide field of solid-state quantum optics, where a cryogenic environment is often a requirement. At a temperature of 4.6 K we obtain a quality factor of $(9.9 \pm 0.7) \times 10^6$. In conjunction with the small mode volume provided by the nanofiber, this cavity can be either used in the coherent dynamics or the fast cavity regime, where it can provide a Purcell factor of up to 15. Our resonator is therefore suitable for significantly enhancing the coupling between light and a large variety of different quantum emitters and due to its proven performance over a wide temperature range, also lends itself for the implementation of quantum hybrid systems.

1. Introduction

Achieving efficient coupling between quantum emitters and light is an important goal of research in quantum communication and computation, sensor applications and fundamental studies. Such an efficient interaction can for example be realized by means of an optical cavity or by reducing the mode area of the light field to the size of the emitter's interaction cross-section. Optical nanofibers offer such a strong transverse confinement of the light field. This makes them a versatile tool for interfacing different types of emitters such as atoms [1–3], single molecules [4], quantum dots [5–7] and color centers in diamond [8,9]. For many proof-of-principle experiments, cold atoms were the emitters of choice as they represent a well-controlled and isolated system. However, the experimental overhead for a cold-atom set-up is significant and solid-state emitters are much more suitable for practical and scalable platforms for quantum networks or nanosensors [10,11].

Yet, the optical transitions of solid state emitters also couple to the phononic degrees of freedom of the system, leading to dephasing and inelastic scattering. In order to avoid this problem, the phonons of the system have to be frozen out and the branching ratio of emission into the coherent zero-phonon line has to be maximized. Further, cryogenic temperatures may be required to be able to spectrally address individual solid state emitters in the case, where many are present in the same host system [4]. This calls for a cryo-compatible optical microresonator with high quality factor, Q, that selectively accelerates the desired optical transition via the Purcell effect [12–15]. Here, we show that a fully fiber-based optical microresonator that consists of a tapered optical fiber with two integrated fiber Bragg gratings (FBGs) [16,17], as demonstrated in [18], can be employed at cryogenic temperatures. In particular, we confirm that a high Q factor prevails after

contact gas-cooling from room temperature to liquid helium temperature. Consequently, the resonator is still compatible with reaching the strong coupling regime. Furthermore, for usage at cryogenic temperatures, the alignment-free character of our resonator represents an advantage over modular resonators which tend to misalign when being cooled down.

2. Experimental methods

To obtain the in-fiber resonator, two FBGs with similar transmission spectra are laser written into a commercial single mode fiber SM800 [19]. Along the fiber, the gratings are separated by 20 mm. In this way, a Fabry-Perot-like resonator for a center wavelength of 852 nm is created [18,20]. To achieve a small mode volume of the resonator and to enable evanescent coupling of quantum emitters to this cavity mode, the fiber section between the two FBGs is tapered using a homebuilt fiber pulling rig [21]. The tapered optical fiber features a nominal waist length of 3 mm and diameter of 500 nm. In the taper section, the weakly guided LP_{01} mode of the standard single mode optical fiber is adiabatically transformed into the strongly guided HE_{11} mode of the nanofiber waist and back and the small waist diameter guarantees single mode operation for wavelengths $\lambda > 691$ nm. After the tapering process, the gratings are separated by 93 mm. In view of the guided resonator modes, this type of cavity is completely alignment-free. To cool the cavity, it is mounted in a copper probe chamber inside a liquid helium bath cryostat. For characterization of the resonator prior to tapering, it is clamped onto a teflon mount. After tapering, the fiber resonator is fixed using Stycast epoxy (Loctite Stycast 2850FT with CAT23LV) onto a silica fiber mount on one side and a piezo element that sits on a copper support on the other side. This method of mounting the resonator in principle enables strain-tuning of the cavity using the piezo. This is however often not a necessary requirement for coupling solid-state emitters to the resonance of a cavity as the emitters often exhibit a large inhomogeneous broadening due to their nanoenvironment and thus a suitable emitter can be picked out from the ensemble [22,23]. First measurements did not show any effect of the piezo, most probably due to insufficient pre-straining of the tapered fiber. If the fiber is pre-strained enough [24] before cool-down, the maximum displacement of the piezo of about 45 μm at liquid helium temperatures is enough to scan the cavity over many free spectral ranges. Alternatively, the piezo can also be mounted on the silica fiber holder directly to avoid any differential length contraction. The fiber mount itself is attached to a copper support with chamfered edges to prevent scratching of the bare optical
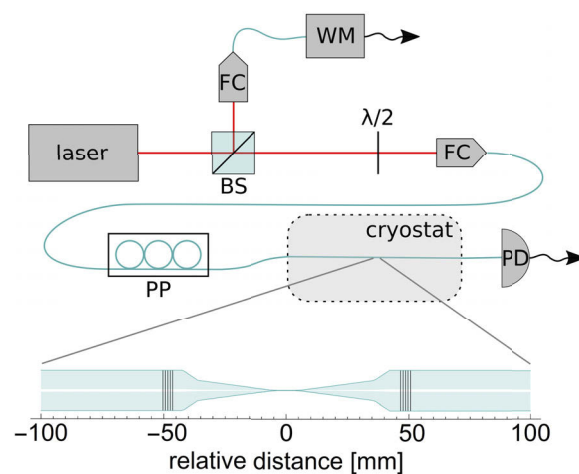

Fig. 1. Optical setup with a closeup of the nanofiber-based resonator; BS - beam splitter, FC - fiber coupler, WM - wavemeter, PP - polarization paddels, PD - photodiode

fiber that could then cause it to break. To achieve efficient cooling of the entire fiber cavity, the probe chamber is slowly evacuated and backfilled with about 50 mbar of helium buffer gas before cool-down. The cryostat is then filled with liquid nitrogen and liquid helium and everything is left to thermalize. The temperature of the sample chamber wall is continuously monitored by a calibrated ruthenium-oxide temperature sensor.

To optically characterize the cavity, a tunable laser (Velocity TLB-6716) is launched into the optical fiber that is led into the cryostat through a teflon feedthrough [25] and spliced to the fiber-based cavity. The transmission of the cavity is measured using a photodiode. Part of the laser beam that is coupled into the optical fiber is split off and coupled into a wavemeter (HighFinesse), which continuously monitors the laser frequency with a relative precision better than 3×10^{-7}. The optical setup is depicted in Fig. 1, where the inset shows a closeup of the nanofiber-based resonator with its nominal radius-profile.

3. Results and discussion

Figure 2 shows the transmission of the cavity covering one free spectral range (FSR) at 4.6 K. As the nanofiber-based resonator is inherently birefringent, the input polarization has to be tuned using polarization paddles such that only one resonance per FSR is observed [18]. The $\lambda/2$-plate (Fig. 1) then enables the selective excitation of the two orthogonal quasi-linearly polarized modes of the resonator. By fitting Airy functions to transmission scans at different laser frequencies, the finesse as a function of frequency is obtained. This procedure is repeated several times and the mean value of the finesse is plotted together with the transmission for a wide wavelength range in Fig. 3. We define the center wavelength of the resonator, λ_c, as the point of best overlap of the reflection bands of the two FBGs and hence, the point of maximum finesse of the resonator.
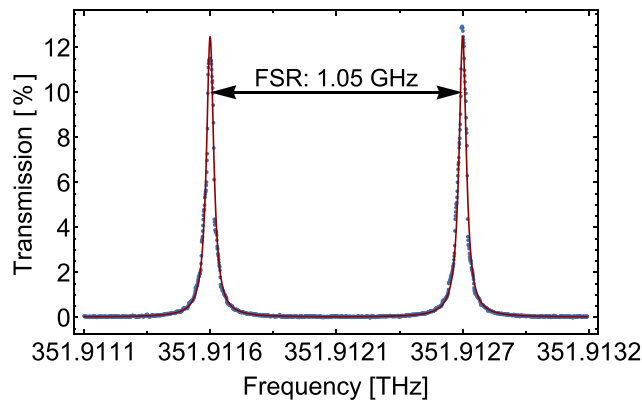

Fig. 2. Transmission spectrum over one FSR including an Airy function fit. The transmission is normalized to the off-resonant transmission outside the stop band.

At a temperature of 4.6 K we measure a maximum finesse of 29.4 ± 1.3 for the nanofiber-based resonator. The spectral position of the corresponding transmission peak corresponds to the center wavelength of the resonator, yielding λ_c = 851.8944 ± 0.0025 nm (ν_c = 351.9127 ± 0.0011 THz), where the error is one FSR. When the FBGs are cooled, thermal contraction and temperature-induced refractive index change cause a shift of the center frequency of the resonator. However, for a stable cavity that shall be on resonance with certain quantum emitters, a good knowledge of the wavelength shift at cryogenic temperatures is crucial. We measure a center wavelength of 852.5555 ± 0.0026 nm at room temperature, and hence a temperature-dependent wavelength shift of −0.6611 ± 0.0051 nm upon cooldown. The room temperature measurements of the center wavelength before cooling down and after warming up the resonator again are shifted
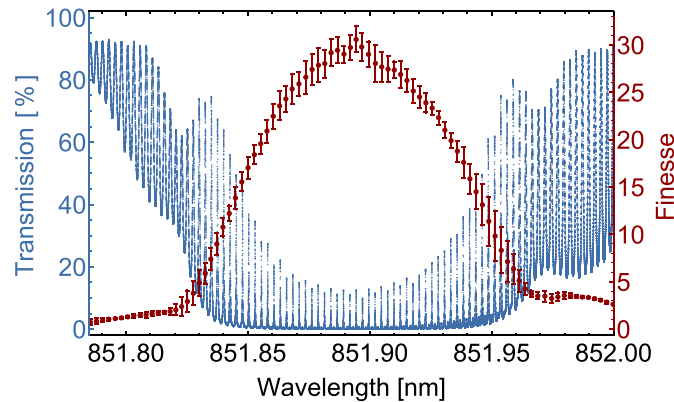
Fig. 3. Transmission and finesse of the nanofiber-based resonator as a function of laser detuning at 4.6 K. The cavity modes show up as transmission peaks within the 0.2 nm wide stop band of the FBGs. The transmission is normalized to the off-resonant transmission outside the stop band.

by 0.0209 nm. Before cooldown we measure a lower maximum finesse of 16.0 ± 0.4 compared to after warming up of the resonator, where a maximum finesse of 31.6 ± 2.5 is measured. The lower finesse value before cooldown may stem from torsion or strain that shifts the reflection band of one of the FBGs a little, leading to a slight shift of the center wavelength and, due to the altered overlap of the two reflection bands, to a lower finesse. The strain associated with the observed wavelenght shift can be calculated [16] to be $\epsilon = 3.1 \times 10^{-5}$. This effect is diminished upon cooldown and we obtain an equally high finesse value at 4.6 K and at room temperature after warming up of the resonator. This means that the shift obtained from these two measurements is solely due to the temperature change and hence this measurement of the temperature-dependent wavelength shift is more reliable for investigating the thermo-optic effect in silica. More details on the temperature-dependent wavelength shift and the thermo-optic coefficient of the FBG resonator can be found in the appendix.

Generally, the tapering process itself can reduce the finesse of the infiber-cavity due to additional taper transmission losses and due to possible thermally induced decrease of the FBGs reflectivities. In our case we measure an initial finesse value of 177.7 ± 26.4 at 4.6 K before tapering the fiber section between the two FBGs. The finesse of the resonator can be written in terms of the FBG reflectivities R_1 and R_2 and a single pass cavity transmission T_c as

$$\mathcal{F} = \frac{\pi \sqrt[4]{R_1 R_2} \sqrt{T_c}}{1 - T_c \sqrt{R_1 R_2}}. \tag{1}$$

Assuming that the propagation losses of the unprocessed fiber are negligible ($T_c = 1$) and that both mirrors have the same reflectivity, we obtain $R = 98\%$ from the measured finesse value. The transmission of a Fabry-Perot cavity with a phase difference δ between consecutive transmitted beams is given by

$$T = \frac{(1 - R_1)(1 - R_2)T_c}{(1 - T_c\sqrt{R_1 R_2})^2} \frac{1}{1 + (2\mathcal{F}/\pi)^2 \sin^2 \delta/2}. \tag{2}$$

For the nanofiber-based resonator at 4.6 K, we measure a finesse of 29.4 and a maximum transmission on resonance of $T/T_c = 0.14$. Solving Eqs. (1) and (2) simultaneously yields a reflectivity per mirror of $R_1 = R_2 = 96\%$ and a nanofiber transmission of $T_c = 93\%$. This is lower than the final nanofiber transmission of 98% monitored during the heat and pull process and may be due to dust that accumulated on the fiber waist. In principle, a higher fiber transmission should be achievable as transmissions of up to 99.95% have been demonstrated [26].

At a temperature of 4.6 K, the maximum finesse of 29.4 in conjunction with an FSR of 1.05 $\pm$ 0.06 GHz, yields a Q-factor of our nanofiber-based resonator of $(9.9 \pm 0.7) \times 10^6$. A figure of merit for the performance of a resonator with respect to the coupling efficiency between the light field and a quantum emitter is the cooperativity $C = g^2/(2\gamma_0\kappa)$, where $2g = \sqrt{2\mu^2\omega/(\hbar\epsilon_0 V)}$ is the single photon Rabi frequency with the dipole moment μ, the effective mode volume V and the free space permittivity ϵ_0. Furthermore, $2\kappa = \omega/Q$ is the cavity decay rate and $2\gamma_0$ the free space spontaneous emission rate of the emitter. g and κ scale with the cavity length L_c as $\propto 1/\sqrt{L_c}$ and $\propto 1/L_c$, respectively, while γ_0 is independent of the cavity length.

Thus, C is independent of L_c and by choosing the cavity length appropriately, a cavity, given $C > 1$, can operate in the coherent dynamics or the Purcell regime [18]. For a two-level emitter, the cooperativity is related to the enhancement of the spontaneous emission by $2C = F_P = 3\lambda^3/(4\pi^2)Q/V$, where F_P is the Purcell factor [27]. Assuming perfect overlap between the dipole moment of an emitter on the surface of the nanofiber and the quasilinearly-polarised field of the nanofiber gives a minimum effective mode volume of $4.9 \times 10^4 \lambda^3$, where the mode volume is the effective mode area [4,28] times the length of the cavity determined by the free spectral range. The mode area is defined as $A_{\text{eff,surf}} = P/(I_{\text{surf}}(\hat{\mathbf{d}} \cdot \hat{\mathbf{e}}_{\text{surf}})^2)$, where I_{surf} is the surface intensity, $\hat{\mathbf{e}}_{\text{surf}}$ the polarization vector at the position of the emitter and $\hat{\mathbf{d}}$ the unit vector of the dipole moment of the solid-state emitter. For a perfect overlap between polarization of the light field and the transition dipole moment of the quantum emitter, the maximum cavity Purcell factor is 15 on the surface of the nanofiber. Assuming an orientation-averaged dipole instead, gives an average cavity Purcell factor of 5. In practice, achieving maximum alignment between the dipole moment of a solid-state emitter in a nano-solid and the polarisation vector of the cavity may prove challenging. However, if an amorphous solid is used [29], the dipole moments of individual emitters differ in direction and the most suitable emitter can be chosen.

When calculating the channeling efficiency into the nanofiber-based cavity in the fast cavity regime, one also has to consider the inherent Purcell enhancement $P_{\text{TOF}} = \gamma_{\text{total}}/\gamma_0$ induced by the optical nanofiber without mirrors [30]. This amounts to 1.57 in our case. Here, the total scattering rate of the emitter $\gamma_{\text{total}} = \gamma_{\text{guided}} + \gamma_{\text{rad}}$, is the sum of the scattering rate to guided modes of the nanofiber without mirrors and to radiation modes. The channeling efficiency for a nanofiber-based cavity is then given by [31]

$$\eta_c = \frac{\eta P_{\text{TOF}} + F_P}{P_{\text{TOF}} + F_P}, \tag{3}$$

where $\eta = \gamma_{\text{guided}}/\gamma_{\text{total}}$ is the channeling efficiency of the optical nanofiber without mirrors. For an orientation-averaged dipole this means that >80% of photons are channeled into the cavity. Hence, this resonator is well-suited for increasing the efficiency of single photon sources of solid state emitters with low emission on the zero phonon line [32–35] and for investigating long-range photon-mediated interactions between different quantum emitters [36].

4. Conclusion

In summary, we present a cryogenic, nanofiber-based microcavity with high quality factors. Together with its small mode volume, this cavity would allow one to significantly increase the coupling between a light field and a quantum emitter by providing a Purcell factor of up to 15. These properties compare very well to those of other micro- [12–14,22,37–42] or nanocavities [15,43]. Moreover, our resonator is fully fiber-integrated and alignment-free. It is therefore suitable for a large variety of emitters [4,44–49] and, thanks to its implementation in a cryogenic environment without any loss in transmission, might also be used for the implementation of quantum hybrid systems [50,51].

5. Appendix: Temperature-dependent wavelength shift of fiber Bragg grating resonators

The temperature-dependent wavelength shift of the FBG's reflection band at an initial Bragg wavelength λ_{B_0} and refractive index n_0 is given by [16,17,52,53]:

$$\frac{\mathrm{d}\lambda_B}{\lambda_{B_0}} = (\alpha + \frac{1}{n_0}\frac{\mathrm{d}n}{\mathrm{d}T})\,\mathrm{d}T, \tag{4}$$

where α denotes the thermal expansion coefficient and $(1/n_0)(dn/dT)$ is the thermo-optic coefficient. In our case, two FBGs form a resonator with a center wavelength λ_c, given by the wavelength of best overlap of the reflection bands of the two FBGs. We approximate $\lambda_{c_0} = (\lambda_{B_{01}} + \lambda_{B_{02}})/2$. Thus, we can apply Eq. (4) for describing the temperature dependence of λ_c. We measure transmission spectra of the nanofiber-based cavity at room temperature and 4.6 K, as shown in Fig. 3. We then evaluate the shift of λ_c. For the nanofiber-based resonator, we find $\lambda_c = 852.5555 \pm 0.0026$ nm and 851.8944 ± 0.0025 nm for the highest finesse values at room temperature and at 4.6 K, respectively. Hence, we measure a shift of -0.6611 ± 0.0051 nm upon cooldown.

Previously, temperature dependence of FBG's reflection bands has mainly been studied in the context of FBG temperature sensors, where the focus lies on maximising sensitivity by coating the FBG or embedding it into other materials with a high thermal expansion coefficient [52–57]. There, the large thermal expansion coefficients of the other materials dominate so that the smaller thermo-optic effect of the FBG itself is less relevant. However, for a silica structure as our nanofiber-based Bragg grating resonator, it is known that the contribution of the thermo-optic effect exceeds that due to thermal expansion [53,58–61] when the structure is cooled from room temperature to liquid helium temperatures. At room-temperature, typical values of the thermal expansion coefficient and the thermo-optic coefficient are 0.55×10^{-6} K^{-1} [16] and 6.29×10^{-6} K^{-1} [53], respectively. It is known that the resulting temperature-dependent wavelength shift decreases with decreasing temperature [54]. We measure a fractional center wavelength-shift of $d\lambda_c/\lambda_c = -(7.8\pm1.7)\times10^{-4}$ for cooling from 295K to 4.6K. As the effect of α on the total wavelength shift is small compared to the thermo-optic effect, we assume α to be constant and obtain a fractional change of the refractive index of $dn/n = -(6.1 \pm 1.7) \times 10^{-4}$. To relate our measurements to previous literature on the thermo-optic coefficient of silica [17,53,62,63], one may consider the temperature averaged thermo-optic coefficient of $\overline{\frac{1}{n_0}\frac{dn}{dT}} = \frac{1}{T_f-T_i}\int_{T_i}^{T_f}\frac{1}{n_0}\frac{dn}{dT}dT = (2.1\pm0.4)\times10^{-6}\,\mathrm{K}^{-1}$ for the temperatures $T_i = 295$ K and $T_f = 4.6$ K, as obtained from our measured shift. The error here is mainly determined by the width of the reflection bands (HWHM $\approx$ 0.1 nm). As the overlap of the FBGs may differ between one cavity to the next, the reflection band width determines the precision, with which we are able to measure the thermo-optic coefficient. The effect of using a temperature-dependent value for α instead as has been measured in [58,59] is less than the given error bar. As a test for our value of the thermo-optic coefficient, we repeat our measurements with a second FBG resonator without a nanofiber-section that has a center wavelength of 852.3305 ± 0.0097 nm at room temperature. We find a shift of -0.7969 ± 0.0190 nm, where the error corresponds to two FSR of the untapered resonator. The corresponding temperature-averaged thermo-optic coefficient is $(2.7 \pm 0.4) \times 10^{-6}$ K^{-1} in good agreement with the first value.

We note that only limited data on thermo-optic coefficients is available for fused silica around 4 K. Some studies [62,63] indicate that the temperature-dependence of the thermo-optic coefficient is also wavelength-dependent. This makes more measurements for different wavelengths and especially down to temperatures of 4 K valuable for all kinds of future experiments.

References

1. E. Vetsch, D. Reitz, G. Sagué, R. Schmidt, S. T. Dawkins, and A. Rauschenbeutel, "Optical Interface Created by Laser-Cooled Atoms Trapped in the Evanescent Field Surrounding an Optical Nanofiber," Phys. Rev. Lett. **104**(20), 203603 (2010).
2. A. Goban, K. S. Choi, D. J. Alton, D. Ding, C. Lacroûte, M. Pototschnig, T. Thiele, N. P. Stern, and H. J. Kimble, "Demonstration of a State-Insensitive, Compensated Nanofiber Trap," Phys. Rev. Lett. **109**(3), 033603 (2012).
3. M. Hafezi, Z. Kim, S. L. Rolston, L. A. Orozco, B. L. Lev, and J. M. Taylor, "Atomic interface between microwave and optical photons," Phys. Rev. A **85**(2), 020302 (2012).
4. S. M. Skoff, D. Papencordt, H. Schauffert, B. C. Bayer, and A. Rauschenbeutel, "Optical-nanofiber-based interface for single molecules," Phys. Rev. A **97**(4), 043839 (2018).
5. R. Yalla, L. K. Fam, M. Morinaga, and K. Hakuta, "Efficient Channeling of Fluorescence Photons from Single Quantum Dots into Guided Modes of Optical Nanofiber," Phys. Rev. Lett. **109**(6), 063602 (2012).
6. M. Fujiwara, K. Toubaru, T. Noda, H. Zhao, and S. Takeuchi, "Highly Efficient Coupling of Photons from Nanoemitters into Single-Mode Optical Fibers," Nano Lett. **11**(10), 4362–4365 (2011).
7. K. M. Shafi, W. Luo, R. Yalla, K. Iida, E. Tsutsumi, A. Miyanaga, and K. Hakuta, "Hybrid system of an optical nanofibre and a single quantum dot operated at cryogenic temperatures," Sci. Rep. **8**(1), 13494 (2018).
8. L. Liebermeister, F. Petersen, A. v. Münchow, D. Burchardt, J. Hermelbracht, T. Tashima, A. W. Schell, O. Benson, T. Meinhardt, A. Krueger, A. Stiebeiner, A. Rauschenbeutel, H. Weinfurter, and M. Weber, "Tapered fiber coupling of single photons emitted by a deterministically positioned single nitrogen vacancy center," Appl. Phys. Lett. **104**(3), 031101 (2014).
9. M. Fujiwara, H. Zhao, T. Noda, K. Ikeda, H. Sumiya, and S. Takeuchi, "Ultrathin fiber-taper coupling with nitrogen vacancy centers in nanodiamonds at cryogenic temperatures," Opt. Lett. **40**(24), 5702 (2015).
10. I. Aharonovich, D. Englund, and M. Toth, "Solid-state single-photon emitters," Nat. Photonics **10**(10), 631–641 (2016).
11. D. D. Awschalom, R. Hanson, J. Wrachtrup, and B. B. Zhou, "Quantum technologies with optically interfaced solid-state spins," Nat. Photonics **12**(9), 516–527 (2018).
12. J. Benedikter, H. Kaupp, T. Hümmer, Y. Liang, A. Bommer, C. Becher, A. Krueger, J. M. Smith, T. W. Hänsch, and D. Hunger, "Cavity-Enhanced Single-Photon Source Based on the Silicon-Vacancy Center in Diamond," Phys. Rev. Appl. **7**(2), 024031 (2017).
13. M. Fujiwara, T. Noda, A. Tanaka, K. Toubaru, H.-Q. Zhao, and S. Takeuchi, "Coupling of ultrathin tapered fibers with high-Q microsphere resonators at cryogenic temperatures and observation of phase-shift transition from undercoupling to overcoupling," Opt. Express **20**(17), 19545–19553 (2012).
14. D. Wang, H. Kelkar, D. Martin-Cano, D. Rattenbacher, A. Shkarin, S. Utikal, T. Götzinger, and V. Sandoghdar, "Turning a molecule into a coherent two-level quantum system," Nat. Phys. **15**(5), 483–489 (2019).
15. M. Kaniber, A. Kress, A. Laucht, M. Bichler, R. Meyer, M.-C. Amann, and J. J. Finley, "Efficient spatial redistribution of quantum dot spontaneous emission from two-dimensional photonic crystals," Appl. Phys. Lett. **91**(6), 061106 (2007).
16. A. Othonos, "Fiber bragg gratings," Rev. Sci. Instrum. **68**(12), 4309–4341 (1997).
17. Z.-S. Guo, J. Feng, and H. Wang, "Cryogenic temperature characteristics of the fiber Bragg grating sensors," Cryogenics **52**(10), 457–460 (2012).
18. C. Wuttke, M. Becker, S. Brückner, M. Rothhardt, and A. Rauschenbeutel, "Nanofiber fabry-perot microresonator for nonlinear optics and cavity quantum electrodynamics," Opt. Lett. **37**(11), 1949–1951 (2012).
19. E. Lindner, C. Chojetzki, S. Brückner, M. Becker, M. Rothhardt, and H. Bartelt, "Thermal regeneration of fiber Bragg gratings in photosensitive fibers," Opt. Express **17**(15), 12523–12531 (2009).
20. S. Kato and T. Aoki, "Stron coupling between a trapped single atom and an all-fiber cavity," Phys. Rev. Lett. **115**(9), 093603 (2015).
21. F. Warken, A. Rauschenbeutel, and T. Bartholomaus, "Fiber Pulling Profits from Precise Positioning-Precise motion control improves manufacturing of fiber optical resonators," Photonics Spectra **42**, 73 (2008).
22. D. Rattenbacher, A. Shkarin, J. Renger, T. Utikal, S. Götzinger, and V. Sandoghdar, "Coherent coupling of single molecules to on-chip ring resonators," New J. Phys. **21**(6), 062002 (2019).
23. M. Gregor, R. Henze, T. Schröder, and O. Benson, "On-demand positioning of a preselected quantum emitter on a fiber-coupled toroidal microresonator," Appl. Phys. Lett. **95**(15), 153110 (2009).
24. S. Holleis, T. Hoinkes, C. Wuttke, P. Schneeweiss, and A. Rauschenbeutel, "Experimental stress-strain analysis of tapered silica optical fibers with nanofiber waist," Appl. Phys. Lett. **104**(16), 163109 (2014).
25. E. Abraham and E. A. Cornell, "Teflon feedthrough for coupling optical fibers into ultrahigh vacuum systems," Appl. Opt. **37**(10), 1762 (1998).
26. J. E. Hoffman, S. Ravets, J. A. Grover, P. Solano, P. R. Kordell, J. D. Wong-Campos, L. A. Orozco, and S. L. Rolston, "Ultrahigh transmission optical nanofibers," AIP Adv. **4**(6), 067124 (2014).
27. D. L. Andrews, ed., *Photonics: Scientific Foundations, Technology and Applications* (Wiley, 2015).
28. F. Warken, E. Vetsch, D. Meschede, M. Sokolowski, and A. Rauschenbeutel, "Ultra-sensitive surface absorption spectroscopy using sub-wavelength diameter optical fibers," Opt. Express **15**(19), 11952 (2007).
29. S. Faez, P. Türschmann, H. R. Haakh, S. Götzinger, and V. Sandoghdar, "Coherent Interaction of Light and Single Molecules in a Dielectric Nanoguide," Phys. Rev. Lett. **113**(21), 213601 (2014).

30. K. Nayak, M. Sadgrove, R. Yalla, F. L. Kien, and K. Hakuta, "Nanofiber quantum photonics," J. Opt. **20**(7), 073001 (2018).

31. F. L. Kien and K. Hakuta, "Cavity-enhanced channeling of emission from an atom into a nanofiber," Phys. Rev. A **80**(5), 053826 (2009).

32. C. Kurtsiefer, S. Mayer, P. Zarda, and H. Weinfurter, "Stable solid-state source of single photons," Phys. Rev. Lett. **85**(2), 290–293 (2000).

33. N. R. Jungwirth, C. B. Y. Ji, M. G. Spencer, M. E. Flatté, and G. D. Fuchs, "Temperature dependence of wavelength selectable zero-phonon emission from single ddefect in hexagonal boron nitride," Nano Lett. **16**(10), 6052–6057 (2016).

34. M. Pototschnig, Y. Chassagneux, J. Hwang, G. Zumofen, A. Renn, and V. Sandoghdar, "Controlling the Phase of a Light Beam with a Single Molecule," Phys. Rev. Lett. **107**(6), 063001 (2011).

35. A. Jeantet, Y. Chassagneux, C. Raynaud, P. Roussignol, J. S. Lauret, B. Besga, J. Estève, J. Reichel, and C. Voisin, "Widely tunable single-photon source from a carbon nanotube in the purcell regime," Phys. Rev. Lett. **116**(24), 247402 (2016).

36. S. Rist, J. Eschner, M. Hennrich, and G. Morigi, "Photon-mediated interaction between two distant atoms," Phys. Rev. A **78**(1), 013808 (2008).

37. A. Faraon, P. E. Barclay, C. Santori, K.-M. C. Fu, and R. G. Beausoleil, "Resonant enhancement of the zero-phonon emission from a colour centre in a diamond cavity," Nat. Photonics **5**(5), 301–305 (2011).

38. J. Gallego, W. Alt, T. Macha, M. Martinez-Dorantes, D. Pandey, and D. Meschede, "Strong Purcell effect on a neutral atom trapped in an open fiber cavity," Phys. Rev. Lett. **121**(17), 173603 (2018).

39. A. W. Schell, H. Takashima, S. Kamioka, M. Oe, Y. Fujiwara, O. Benson, and S. Takeuchi, "Highly efficient coupling of nanolight emitters to a ultra-wide tunable nanofibre cavity," Sci. Rep. **5**(1), 9619 (2015).

40. K. Srinivasan and O. Painter, "Optical fiber taper coupling and high-resolution wavelength tuning of microdisk resonators at cryogenic temperatures," Appl. Phys. Lett. **90**(3), 031114 (2007).

41. T. Herzog, M. Sartison, S. Kolatschek, S. Hepp, A. Bommer, C. Pauly, F. Mücklich, C. Becher, M. Jetter, S. L. Portalupi, and P. Michler, "Pure single-photon emission from in(ga)as qds in a tunable fiber-based external mirror microcavity," Quantum Sci. Technol. **3**(3), 034009 (2018).

42. R. Henze, J. M. Ward, and O. Benson, "Temperature independent tuning of whispering gallery modes in a cryogenic environment," Opt. Express **21**(1), 675–680 (2013).

43. D. Englund, A. Faraon, I. Fushman, N. Stoltz, P. Petroff, and J. Vučković, "Controlling cavity reflectivity with a single quantum dot," Nature **450**(7171), 857–861 (2007).

44. M. E. Trusheim, B. Pingault, N. H. Wan, M. Gundogan, L. De Santis, K. C. Chen, M. Walsh, J. J. Rose, J. N. Becker, B. Lienhard, E. Bersin, G. Malladi, D. Lyzwa, H. Bakhru, I. Walmsley, M. Atature, and D. Englund, "Transform-limited photons from a tin-vacancy spin in diamond," arXiv:1811.07777 (2019).

45. J. Görlitz, D. Herrmann, G. Thiering, P. Fuch, M. Gandil, T. Iwasaki, T. Taniguchi, M. Kieschnick, J. Meijer, M. Hatano, A. Gali, and C. Becher, "Spectroscopic investigations of negatively charged tin-vacancy centres in diamond," arXiv:1909.09435 (2019).

46. A. N. Vamivakas, Y. Zhao, C.-Y. Lu, and M. Atatüre, "Spin-resolved quantum-dot resonance fluorescence," Nat. Phys. **5**(3), 198–202 (2009).

47. S. Pazzagli, P. Lombardi, D. Martella, M. Colautti, B. Tiribilli, F. S. Cataliotti, and C. Toninelli, "Self-assembled nanocrystals of polycyclic aromatic hydrocarbons show photostable single-photon emission," ACS Nano **12**(5), 4295–4303 (2018).

48. A. Dietrich, M. Bürk, E. S. Steiger, L. Antoniuk, T. T. Tran, M. Nguyen, I. Aharonovich, F. Jelezko, and A. Kubanek, "Observation of fourier transform limited lines in hexagonal boron nitride," Phys. Rev. B **98**(8), 081414 (2018).

49. D. Serrano, J. Karlsson, A. Fossati, A. Ferrier, and P. Goldner, "All-optical control of long-lived nuclear spins in rare-earth doped nanoparticles," Nat. Commun. **9**(1), 2127 (2018).

50. S. Minniberger, F. Diorico, S. Haslinger, C. Hufnagel, C. Novotny, N. Lippok, J. Majer, C. Koller, S. Schneider, and J. Schmiedmayer, "Magnetic conveyor belt transport of ultracold atoms to a superconducting atomchip," Appl. Phys. B **116**(4), 1017–1021 (2014).

51. R. J. Schoelkopf and S. M. Girvin, "Wiring up quantum systems," Nature **451**(7179), 664–669 (2008).

52. T. Mizunami, H. Tatehata, and H. Kawashima, "High-sensitivity cryogenic fibre-bragg-grating temperature sensors using teflon substrates," Meas. Sci. Technol. **12**, 914 (2001).

53. M. B. Reid and M. Ozcan, "Temperature dependence of fiber optic bragg gratings at low temperatures," Opt. Eng. **37**(1), 237–240 (1998).

54. T. Habisreuther, W. Hailemichael, E. Ecke, I. Latka, C. Schröder, K. Chojetzki, K. Schuster, M. Rothhardt, and R. Willsch, "Ormocer coated fiber-optic bragg grating sensors at cryogenic temperatures," IEEE Sens. J. **12**(1), 13–16 (2012).

55. M. Yamada, Y. Tanaka, M. Ogata, K. Mizuno, K. Nagashima, S. Okumura, and Y. Terada, "Measurement and improvement of characteristics using optical fiber temperature sensor at cryogenic temperatures," Phys. C **471**(21-22), 1570–1575 (2011).

56. M. Frovel, A. Guemes, and J. Pintado, "Multiplexable fiber bragg grating temperature sensors embedded in cfrp structures for cryogenic applications," *Proc. 3rd EWSHM*, p. 938–947 (Jul.5-7 2006).

57. S. Gupta, T. Mizunami, T. Yamao, and T. Shimomura, "Fiber bragg grating cryogenic temperature sensor," Appl. Opt. **35**(25), 5202–5205 (1996).
58. G. K. White, "Thermal expansion of vitreous silica at low temperatures," Phys. Rev. Lett. **34**(4), 204–205 (1975).
59. G. K. White, "Thermal expansion of reference materials: copper, silica and silicon," J. Phys. D: Appl. Phys. **6**, 2070–2078 (1973).
60. O. Arcizet, R. Riviére, A. Schliesser, G. Anetsberger, and T. J. Kippenberg, "Cryogenic properties of optomechanical silica microcavities," Phys. Rev. A **80**(2), 021803 (2009).
61. Y. Park and H. Wang, "Regenerative pulsation in silica microspheres," Opt. Lett. **32**(21), 3104–3106 (2007).
62. D. B. Leviton and B. J. Frey, "Temperature-dependent absolute refractive index measurements of synthetic fused silica," Proc. SPIE **6273**, 62732K (2006).
63. G. M. H. Flockhart, R. R. J. Maier, J. S. Barton, W. N. MacPherson, J. D. C. Jones, K. E. Chisholm, L. Zhang, I. Bennion, I. Read, and P. D. Foote, "Quadratic behavior of fiber Bragg grating temperature coefficients," Appl. Opt. **43**(13), 2744–2751 (2004).